https://doi.org/10.1590/1678-992X-2023-0219

ISSN 1678-992X

SCIENTIA AGRICOLA

Research article

Precipitation of amorphous iron and aluminum during the weathering of rock dust in soil columns

Rafael Cipriano da Silva[1]*, Clécia Cristina Barbosa Guimarães[1], Antonio Carlos de Azevedo[2], Marcelo Rodrigo Alves[3], José Alexandre Melo Demattê[2]

[1]Fundação Cearense de Meteorologia e Recursos Hídricos, Av. Rui Barbosa, 1246 – 60115-221 – Fortaleza, CE – Brasil.
[2]Universidade de São Paulo/ESALQ – Depto. de Ciência do Solo, Av. Pádua Dias, 11 – 13418-900 – Piracicaba, SP – Brasil.
[3]Universidade do Oeste Paulista/Faculdade de Agronomia, R. José Bongiovani, 700 – 19050-920 – Presidente Prudente, SP – Brasil.
*Corresponding author <rafael.cipriano@funceme.br>

Edited by: Flávio Henrique Silveira Rabêlo

Received September 19, 2023
Accepted February 21, 2024

ABSTRACT: The application of rock dust (RD) in agricultural soils has shown the capacity to improve soil conditions for plant growth. However, the successful use of RD requires understanding its effects on weathering in soil surfaces and its possible products. In this study, we present the results of an exploratory test in which a RD had its weathering intensified in a soil column by temperature (45 °C) and intense leaching (1,339.2 mm in 24 weeks), in the absence of plants. There was a significant increase in amorphous phases of iron (Fe) and particularly of aluminum (Al) to the amount of 0.13 g kg^{-1} for Fe and 0.16 g kg^{-1} for Al in the 0-0.05 m layer of the column and 0.22 g kg^{-1} for Al in the 0.05-0.10 m layer. These values account for 6 % of the total Fe, and 27 % of the total Al added as RD in the column. Spectral features in the visible-near infrared-short wave infrared (VIS-NIR-SWIR) and mid-infrared (MIR) range, as well as X-ray diffraction (XRD) scans, were inconclusive because of the small signal-noise ratio of the newly precipitated phases. Selective chemical methods targeted to specific soil pools (precipitated, adsorbed, and leached) were more sensitive to capture the new amorphous phases resulting from the RD dissolution. This study contributes to understanding the effects of RD on the availability of ions and the possibility of amorphous oxides precipitating in the soil. In addition, it helps identify other effects associated with using RD, such as changes in the pH, cation exchange capacity (CEC), and nutrient availability.
Keywords: aluminum oxide, enhanced weathering, iron oxide, rock powder

Introduction

Precipitation of iron (Fe) and aluminum (Al) phases with short-range crystallinity, usually referred to as amorphous phases, occurs as one of the first evidence of weathering of mafic rocks (Lewis et al., 2021; Silva et al., 2021; Vienne et al., 2022). These phases may form complexes with organic materials, increase both the cation and anion exchange capacity of the soil (CEC and AEC), adsorb soil phosphorus, silicon, and potentially toxic metals (such as arsenic and chromium), increase the soil aggregate stability, among other effects (e.g., Park et al., 2024; Vienne et al., 2022). When a Fe-rich mafic rock is applied to soil as rock dust (RD), its specific surface area accelerates the rate of mineral weathering, a mechanism known as enhanced rock weathering (ERW) (Swoboda et al., 2022).

The Fe and Al amorphous phases resulting from ERW of mafic RD may increase both the amount and the residence time of soil organic carbon, contributing to atmospheric carbon (C) capture (Fisher et al., 2022; Lewis et al., 2021; Vienne et al., 2022; Wang et al., 2019). For example, Slessarev et al., 2021 showed that the soil weathering rate, rather than the soil weathering state, is the main driver for C capture through the mineral-organic complex path. Consequently, in addition to a significant weathering rate, soils also requires freshly weatherable minerals to provide sources of Fe and Al to precipitate amorphous mineral phases capable of complexing the organic counterparts. Therefore, weathered soils, such as tropical Oxisols, may have their source of weatherable minerals exhausted despite the high weathering rates (Swoboda et al., 2022), diminishing or halting their capacity to produce mineral-organic complexes. Oxisols cover about 2.7 million km^2 (32 %) of the Brazilian territory (Santos et al., 2011). Brazil is the world's fifth largest country in agricultural land area (FAO, 2021) and the largest silicate-carbon sink in the world (Zhang et al., 2021) therefore with a significant potential for C capture through the ERW of RD.

In this experiment, articulated with field plots in a crop farm, we intensively leached soil columns without plants, to detect the rapid precipitation of Fe and Al amorphous oxides. We hypothesized that amorphous Fe and Al precipitation is favored after the weathering of minerals from mafic RD applied in an Oxisol. The objective was to investigate the potential of RD to produce amorphous mineral phases.

Materials and Methods

Characterization of rock dust

The diabase rock dust (RD) came from a quarry in the Limeira Sill, São Paulo State, Brazil (22°36′31″ S, 47°21′45″ W, altitude 529 m). This sill is part of the Serra Geral Formation, which is one of the largest igneous rock provinces in the world, encompassing 1.2 million km^2 and 800,000 km^3 of extrusive rocks (Frank et al., 2009; Lino et al., 2018). The RD was sampled and quartered

from the same 5 Mg (megagram) load applied in a field experiment described by Silva et al. (2017). The total chemical composition of the soil and the RD content was determined by fusion with $LiBO_2/Li_2B_4O_7$ at 1,000 °C, cooled down to a solid disk, and further dissolved in an HNO_3 + HCl solution in which the elements were determined by inductively coupled plasma optical emission spectrometry (ICP-OES) (Table 1).

The XRD analysis was carried out in a MiniFlex II benchtop diffractometer using CuKα radiation (30 kV and 15 mA) and equipped with a Ni filter, a NaI scintillator, and a graphite monochromator. The RD had plagioclase, pyroxenes, magnetite, and ilmenite, which agrees with the description of Lino and Vlach (2021), who studied the Limeira Sill magmatic differentiation. The RD particle size distribution was determined using the same procedure for soils (see below). The RD particle size distribution was 30 g kg^{-1} gravel (> 2,000 µm), 800 g kg^{-1} sand (2,000-50 µm), 160 g kg^{-1} silt (50-2 µm) and 10 g kg^{-1} clay (< 2 µm).

Soil characterization

The soil in the columns was an Anionic Acrudox (Soil Taxonomy; Soil Survey Staff, 1999) collected at a depth of 0-0.10 m in the municipality of Pirassununga, São Paulo State, Brazil (21°58′52.3″ S, 47°22′44.3″ W, altitude 529 m). An aliquot of this Anionic Acrudox was subjected to chemical and physical analyses before the experiment and labeled as a "reference".

At the time of collection, the soil was recently fertilized with 20-05-19 nitrogen-phosphorus-potassium (NPK) at a dose of 380 kg ha^{-1} applied on the surface without plowing (no-till system). The soil was collected right next to the plots used by Silva et al. (2017) in a field experiment with the same RD. The sampled soil was air-dried, crushed, and sieved through a 4-mm sieve.

Soil fractions were obtained by dispersing the sample with NaOH 0.5 mol L^{-1}. The sand was sieved out, dried, weighed, and saved. The clay fraction was estimated by the densimeter method and siphoned after silt decanted, according to the Stokes equation (Day, 1965; Soil Survey Staff, 2014). The particle size distribution of the control soil (Anionic Acrudox) was 800 g kg^{-1} sand, 30 g kg^{-1} silt and 170 g kg^{-1} clay, classified as sandy-loam texture. The sand and silt fractions were XRD scanned in powder mounts (Figure 1A and B, respectively), while the clay fraction was mounted in oriented slides (Figure 1C) in the same diffractometer setup as described for the RD sample.

The experiment

This experiment is part of a series of exploratory tests made in the context of a crop field experiment in the municipality of Pirassununga, São Paulo state, Brazil (Silva et al., 2017). We made columns 0.15 m in height and 0.125 m in diameter by cutting polyvinyl chloride (PVC) pipes. The PVC lid that sealed the bottom of the column had a 0.015 m hole fitted with a plastic tube to collect the leachate. The columns were filled with 1,663 g of soil material to a height of 0.10 m and a soil density of 1.36 kg m^{-3}.

Treatment T0 was the control, and treatment T1 received 15 Mg ha^{-1} of the RD on its surface in order to match conditions of the concurrent field experiment (Silva et al., 2017). Each treatment had four replications. Deionized water was applied weekly at 670 mL (equivalent to a 55.8 mm rainfall). The total water volume applied after six months (24 weeks) was 1,339.2 mm, almost equal to the mean annual precipitation in the soil sampling site (1,470 mm yr^{-1}). The columns were

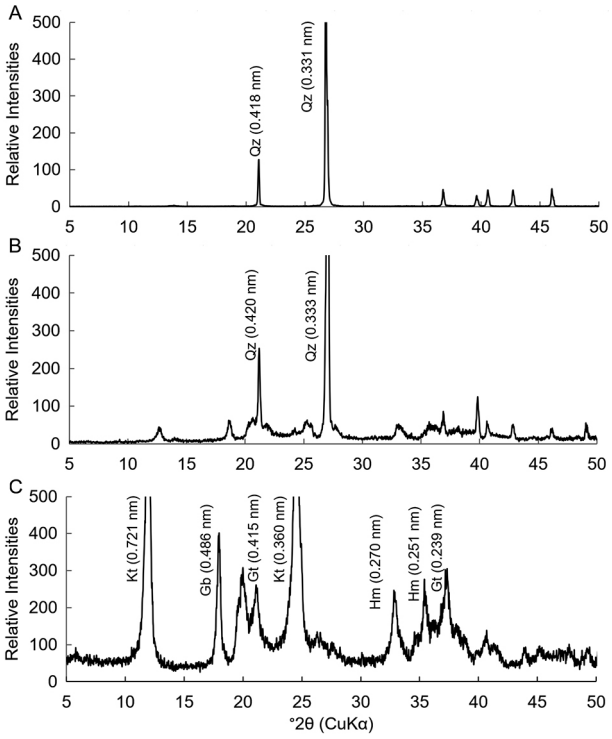

Figure 1 – X-ray diffraction patterns of the A) sand; B) silt; and C) clay fractions of soil used in the columns. Qz = quartz; Kt = kaolinite; Gb = gibbsite; Gt = goethite; Hm = hematite.

Table 1 – Elemental composition of the soil and the rock dust (RD).

	SiO_2	Fe_2O_3	Al_2O_3	CaO	MgO	Na_2O	K_2O	TiO_2	MnO	P_2O_5	LOI	Total
	%											
RD	52.10	14.45	11.90	6.94	3.45	3.06	1.59	3.27	0.24	0.75	1.67	99.55
Soil	92.00	5.27	7.06	0.03	0.04	0.01	0.03	2.53	0.03	0.07	5.25	102.00

LOI = loss on ignition.

kept in an oven at 45 °C, except during the leaching events. No plants were used in this experiment.

The leaching solutions were collected in plastic bottles previously cleaned with 10 % nitric acid (Laxen and Harrison, 1981). The temperature, the pH, and electrical conductivity (EC) were immediately measured after collecting the leachate solution. The solutions were then spiked with drops of 65 % nitric acid to reach pH 2, and refrigerated for further analysis.

Leachate and soil analyses

The concentrations of aluminum (Al), calcium (Ca), iron (Fe), potassium (K), magnesium (Mg), manganese (Mn), sodium (Na), phosphorus (P), and silicon (Si) (mg L^{-1}) were measured directly in the leached solutions using ICP-OES. The total mass of the leached elements was estimated using the Eq. (1):

$$Mel = \sum_{n=1}^{24} C_{el} \times V_l \quad (1)$$

where: M_{el} is the total mass of the leached element (*el*) after 24 weeks (mg); C_{el} is the concentration of element (*el*) in the weekly leachate solution (mg L^{-1}); and V_l is the weekly volume leached (*l*).

After 24 weeks, the columns were disassembled into two layers: 0 to 0.05 m and 0.05 to 0.10 m depths. The soil material was air-dried and gently crushed to pass a 2 mm sieve. The soil fertility analyses were conducted according to protocols prescribed by the state of São Paulo (van Raij et al., 2001). A 2.5 cm^3 soil sample was suspended for 16 h with an amphoteric exchange resin in deionized water. The exchangeable Ca, K, Mg, and P were eluted from the resin with a HCl 0.1 mol L^{-1} + NaCl 1 mol L^{-1} solution. Ca, K, and Mg were measured by atomic absorption spectrometry (AAS) and P by colorimetry. The soil pH was measured in a 1:10 soil using 0.01 mol L^{-1} $CaCl_2$ solution ratio. The potential cation exchange capacity (CEC) was estimated by the sum of the exchangeable content of Ca, Mg, K, and H + Al. The compulsive method measured the effective CEC (CEC_{ef}), which uses a single extraction solution ($BaCl_2$) rather than the sum of the ions. This method is considered more suitable for advanced weathered soils and is not influenced by the RD dissolution in the aliquot (Gillman, 1979; Santos et al., 2024).

The oxides with short-range crystallinity (amorphous) were determined by dissolution in a 0.2 mol L^{-1} ammonium oxalate (AO) solution at pH 2 in darkness (Schwertmann, 1964). The pedogenic iron oxides were measured in a dithionate-citrate-bicarbonate (DCB) solution (Mehra and Jackson, 1958). The RD alone was also subjected to extraction by AO and DCB to account for the direct contribution of RD grains in the T1 soil treatment. The amount of Fe and Al extracted was estimated considering the dilution of the RD in soil. Therefore, the values of Fe and Al (both AO and DCB) in Table 2 for the T1 treatment were corrected for this contribution. The Fe and Al in the AO and DCB extracts were measured by Atomic Absorption Spectrometry (AAS).

The spectral analyses within the range of 350-2,500 nm (visible-near infrared-short wave infrared, VIS-NIR-SWIR) were performed in a Fieldspec Pro spectroradiometer (Analytical Spectral Devices) in the clay fraction of the soil samples of the 0 to 0.05 m layer. The sensor was placed 0.08 m above the sample under two 50 W halogenic lamps, producing a noncollimated beam 0.35 m from the sample at a zenith angle of 30°. A white spectralon ($BaSO_4$) plate was used as the standard to calibrate the spectrometer.

Spectral data from 2,500 to 16,000 nm (MIR) was obtained from the clay samples (0-0.05 m layer) without Fe oxides (DCB-treated; Mehra and Jackson, 1958) using an alpha sample compartment RT-DLaTGS ZnSe (Bruker Optik GmbH) sensor coupled with a drift to acquire the diffuse reflectance. The sensor used a helium-neon (HeNe) laser as a light source and the calibration standard at each wavelength. The spectra had a 1.2 nm resolution at 32 scans per second. A gold plate was used as the reference.

The Lilliefors test for data normality and the Cochran and Bartlett test (homogeneity of variances) were applied to the soil analyses results. Verifying normal distribution, the mean tests were performed using the Bonferroni test at a 5 % probability using Sisvar version 5.3 software.

Results

The amounts of Fe and Al extracted directly from the RD by the AO and DCB were measured (Table 2). The amounts were adjusted to the dilution of the RD in the soil 0-0.05 m layer, accounting for 0.04 g kg^{-1} of Fe determined by AO extract (Fe_o) and 0.007 g kg^{-1} of Al by AO (Al_o) (Table 2). These amounts were already subtracted from the results from T0 and T1 in Table 2. The Fe and Al contents in the DCB extract were greater than in the AO extract because DCB dissolves both amorphous and crystalline pedogenic Fe and Al oxides (Fe_d and Al_d). The application of RD in the soil had no effect in Fe_d and Al_d.

The amounts of Fe extracted with AO, Fe_o, in T1 at 0-0.05 m (0.69 g kg^{-1}) and Al_o, in both depths, 0-0.05 and 0.05-0.10 m (1.18 g kg^{-1} and 1.23 g kg^{-1}), were greater than in the control (T0) (Table 2). In addition, Al_o was greater than the amount of Fe_o. The increase of Fe_o precipitated in the 0-0.05 m depth in T1 was 0.13 g kg^{-1} (0.69 g kg^{-1} – 0.56 g kg^{-1}), and for Al_o, 0.16 g kg^{-1} at the 0-0.05 m layer and 0.22 g kg^{-1} in the 0.05-0.10 m layer. Converting these values for the column layers (834.5 g of soil at each 0-0.05 m column layer) during the experiment, the significant amounts of amorphous phases produced were Fe_o 0.11 g per column (0-0.05 m layer) and Al_o was 0.13 g per column (0-0.05 m) plus 0.18 g per column (0.05-0.10 m) totaling 0.31 g per

column. Considering the application of 18.40 g RD per column (equivalent to 15 Mg ha^{-1}) and the total content of Fe (Fet , 1.86 g) and Al (Alt, 1.16 g) (Table 1), the total concentration of iron (Fe_t) is 6 % into $Fe_{o0\text{-}0.05\ m}$ and 27 % of Al_t into $Al_{o0\text{-}0.10\ m}$.

The total Ca, Mg, and Na leached in T1 was greater than in T0 (Table 3). In the soil (Table 4), all exchangeable ions decreased during the experiment (compared to the reference soil analysis), except for Mg in both T0 and T1. In T1, the amount of Ca leached was about two-fold that of Mg, resulting in depletion of the exchangeable Ca to concentrations below the reference soil, but with an increase of exchangeable Ca at 0.05-0.10 m layer. Although T1 showed an increase in total Mg and Na leached, the increase was not observed in Mg and Na exchangeable.

The total K leached was about 100 mg (about 2.6 $mmol_c$) 24 weeks (Table 3), much higher than the other elements, and is close to the depletion of K exchangeable as compared to the control soil (from 7 to about 3 $mmol_c$ dm^{-3}, Table 4). The high exchangeable and leached K values were related to the K fertilizer previously applied in the farm field. In addition, the slight increase in the more mobile ions (K and Na exchangeable) at the 0-0.05 m layer may be related to the increase in the upward flow of soil solution, augmented by the high evaporation rate inside the oven.

There was no difference between treatments for total Al, Fe, and Si leached. Nevertheless, a more significant amount of leached Al and Fe was observed in T1 during the first three weeks (Figure 2A and B). Despite the abundance of the Si solid phases in RD (Table 1 and Figure 1A and B), the total amount of Si leached was similar in both treatments, approximately 16 mg; however, there was an increase of exchangeable Si at 0-0.05 m layer in T1 (Table 4). The total P leached was greater in T0 (2.3 g) as compared to T1 (1.7 mg) (Table 3), while the P available increased T1 at 0-0.05 m layer.

The pH of the leached solutions fluctuated mainly between pH 6.0 and pH 6.4 (Figure 2C). In the soil, there was no difference in the pH after 24 weeks. Since the soil mineralogy indicates the dominance of pH-dependent charges (oxides and kaolinite; Figure 1C), the lack of difference in CEC values (both potential and effective) was expected because of the buffering capacity of the

Table 2 – Average Fe and Al extracted with dithionate-citrate-bicarbonate (Fe_d and Al_d) and ammonium oxalate (Fe_o and Al_o) solutions. The contribution of Fe and Al extracted directly from the RD was already subtracted from T1 results.

Treatments	Soil layers	Fe_o	Fe_d	Al_o	Al_d	Fe_o/Fe_d
	m	---------- g kg^{-1} ----------				
RD	-	1.73	3.51	0.31	1.58	0.49
T0	0-0.05	0.56 b	19.40 a	1.02 b	4.05 a	0.03 b
	0.05-0.10	0.56 b	20.74 a	1.01 b	4.00 a	0.03 b
T1	0-0.05	0.69 a	19.29 a	1.18 a	4.56 a	0.04 a
	0.05-0.10	0.61 b	20.08 a	1.23 a	4.31 a	0.03 b
CV %		6	6	6	13	5

Same letters in the column = no statistical difference at 5 % by the Bonferroni test; CV % = coefficient of variation. T0 = control; T1 = 15 Mg ha^{-1} of rock dust; RD = rock dust. Fe = iron; Al = aluminum.

Table 3 – Average total mass of elements (M_{el}) in the leachate after 24 weeks.

Treatments	Ca	Mg	K	Al	P	Na	Si	Fe
	---------- M_{el} (mg) ----------							
T0	28.9 b	14.1 b	102.1 a	1.7 a	2.3 a	1.8 b	15.8 a	0.7 a
T1	37.7 a	17.5 a	109.0 a	2.1 a	1.7 b	4.5 a	16.0 a	0.9 a
CV %	16	14	9	43	13	14	18	44

Same letters in the column = no statistical difference at 5 % by the Bonferroni test; CV % = coefficient of variation. T0 = control; T1 = 15 Mg ha^{-1} of rock dust. Ca = calcium; Mg = magnesium; K = potassium; Al = aluminum; P = phosphorus; Na = sodium; Si = silicone; Fe = iron.

Table 4 – Average values of pH and exchangeable elements after 24 weeks in the soil columns.

Treatments	Layer	pH	Ca	Mg	K	Al	CEC	CEC_{ef}	P	Na	Si	Fe
	m		---------- $mmol_c$ dm^{-3} ----------					$mmol_c$ kg^{-1}	---------- mg dm^{-3} ----------			
Reference*	0-0.10	4.6	9	0.7	7	2	44.0	20.2	47	8	6.5	26
T0	0-0.05	4.6 a	4 b	1.2 a	3.9 a	2 a	40.9 a	18.9 a	33 b	7 a	6.5 ab	23 a
	0.05-0.10	4.6 a	6 b	1.6 a	3.1 b	2 a	38.2 a	19.5 a	34 b	6 a	6.1 b	24 a
T1	0-0.05	4.7 a	5 b	1.3 a	3.4 ab	2 a	37.2 a	20.0 a	53 a	8 a	7.4 a	24 a
	0.05-0.10	4.5 a	12 a	1.7 a	2.3 c	2 a	45.3 a	20.2 a	31 b	6 a	5.9 b	26 a
CV %		2	25	22	10	18	10	6	33	15	7	9

*Soil analysis before the experiment. Same letters in the column = no statistical difference at 5 % by the Bonferroni test; CV % = coefficient of variation. T0 = control; T1 = 15 Mg ha^{-1} of rock dust. Ca = calcium; Mg = magnesium; K = potassium; Al = aluminum; CEC = cation exchange capacity; CEC_{ef} = cation exchange capacity effective; P = phosphorus; Na = sodium; Si = silicon; Fe = iron.

system. The EC was greater until the 12th week, roughly mirroring leaching amounts of Fe and Al (Figure 2D). However, while the amount of Fe and Al leached was the highest during the first three weeks, the EC peaked at the fourth and fifth weeks. This suggests that different ions alternate to cause the increase in the EC readings.

The XRD scans of the soil showed the presence of goethite, hematite, and possibly ferrihydrite as the Fe oxide phases (Figure 3A). Kaolinite and gibbsite were also identified. Due to the resolution of the routine XRD and the great dilution of RD in soil (1 to 680, considering the application of 1.36 kg m^{-3} and 0-0.05 m layer), changes in the XRD patterns were not expected and, in fact, were not observed.

The MIR spectral signals (absorption features) associated to Fe oxides (hematite and goethite) in soils were identified mainly between 400 and 700 nm (Coblinski et al., 2020; Coblinski et al., 2021; Ramaroson et al., 2018; Terra et al., 2018) (Figure 4). The less concave shape of the spectrum near 500 nm suggests the dominance of hematite in the control sample (T0). At the same time, the more pronounced concavity in the T1 curve is related to the greater content of the goethite-like phase than hematite. However, the smaller reflectance in the spectral curve at 450 nm can be associated to goethite (Coblinski et al., 2020). Furthermore, the lower shoulder near 700 nm, associated to the higher absorbance in 920 nm, also suggests that the goethite-like phase content increased in T1 (Coblinski et al., 2021; Terra et al., 2018). In addition, the decrease in the clay fraction albedo in T1 up to 0.1 unit also implies some mineralogical change in the Fe oxides (Baldridge et al., 2009).

The spectral signals of gibbsite ($Al(OH)_3$) were associated to the feature near 2,260 nm, which is attributed to the Al-OH bend (Coblinski et al., 2021; Ramaroson et al., 2018; Terra et al., 2018). This feature *per se* did not change between treatments; nevertheless, it seems to have a different ratio to the kaolinite feature at 2,200 nm, suggesting a change in their relative amount (Figure 4). In addition, the peak associated to the presence of illite is in 2,198-2,206 nm, suggests a possible interference between kaolinite and illite (Ramaroson et al., 2018).

The MIR spectral curve (Figure 5) showed an increase in T1 absorbance at 9,500 nm (relative Al-O and Al-H stretching), which can be interpreted as an increase in the Al (hydro)oxide content. It also promotes a decrease in the reflectance at higher wavelengths (Coblinski et al., 2020). The several bands observed at approximately 7,000 and 8,000 nm are associated to the vibration of Al-O and Si-O bonds. Those between 9,000 and 14,000 nm, are mainly associated with the plagioclases and vibration of H-O-Fe bound in the silicates (pyroxene and amphibole) (Guimarães et al.,

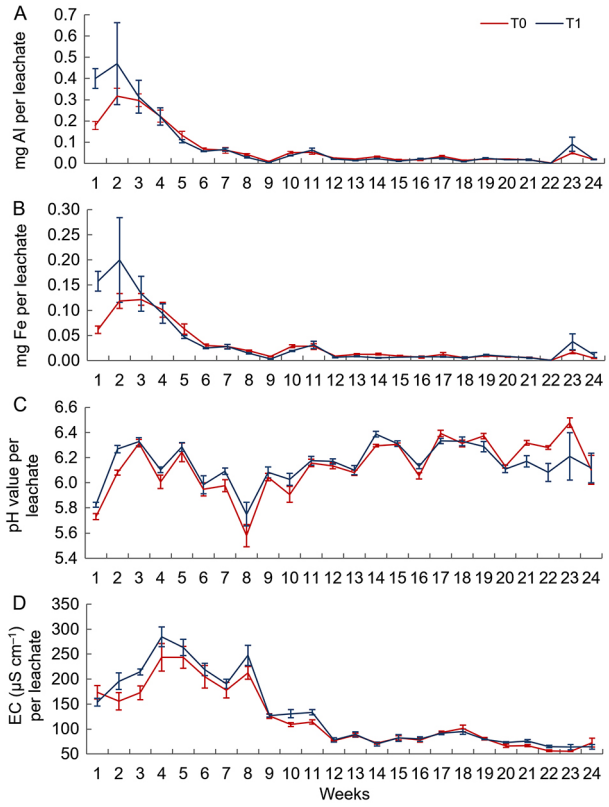

Figure 2 – A) Contents of Aluminum (Al) and B) iron (Fe), C) pH and D) electrical conductivity (EC) values, along the leaching events in the soil columns. T0 = control; T1 = 15 Mg ha^{-1} of rock dust. The bars mean the standard error.

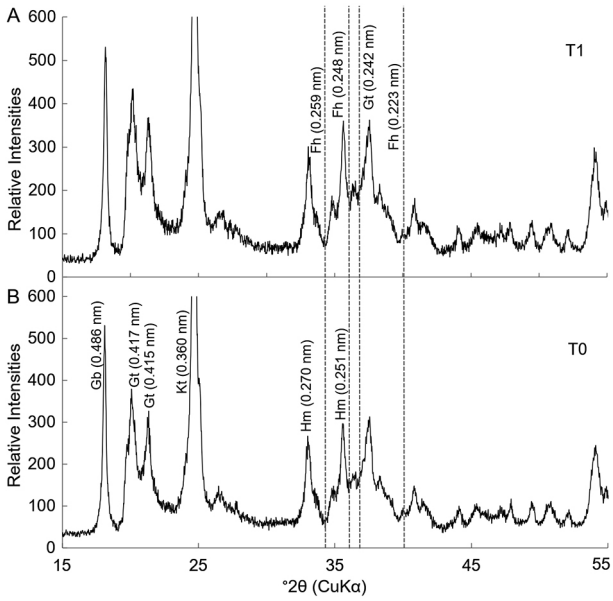

Figure 3 – X-ray diffraction patterns of clay fraction K saturated clay slides. Samples colleted at the end of the experiment, in the, 0-0.05 m layer after 24 weeks of leaching. A) T1 = 15 Mg ha^{-1} of rock dust; B) T0 = control. Fh = ferrihydrite; Gb = gibbsite; Gt = goethite; Hm = hematite; Kt = kaolinite.

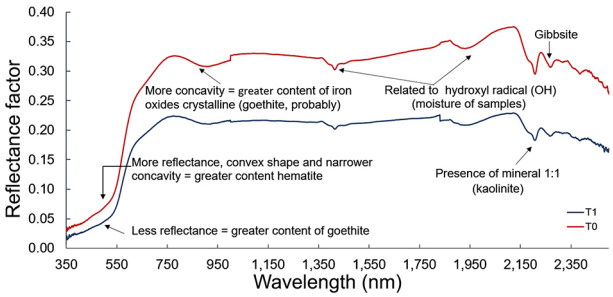

Figure 4 – Comparison of the diffuse reflectance of visible-near infrared-short wave infrared spectral curve in clay fraction of the samples, 0-0.05 m layer after 24 weeks of leaching. T0 = control; T1 = 15 Mg ha^{-1} of rock dust.

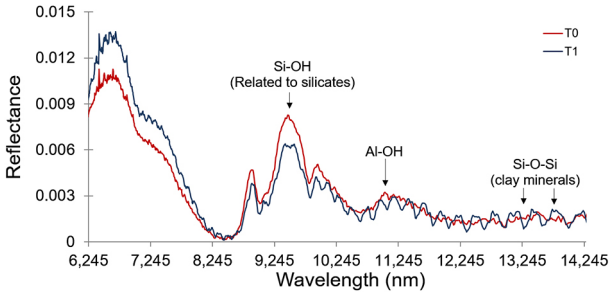

Figure 5 – Comparison of the diffuse reflectance mid infrared spectral curve of the clay fraction, dithionate-citrate-bicarbonate treated. Sample from 0-0.05 m layer after 24 weeks of leaching. T0 = control; T1 = 15 Mg ha^{-1} of rock dust. Al-OH = aluminum-hydroxyl bond; Si-O-Si = silicon-oxygen-silicon bond; Si-OH = silicon-hydroxyl bond.

2021; Hahn et al., 2018; Mohanty et al., 2016). These bands overlapped and masked Al oxide features along the MIR range (Coblinski et al., 2020) and can indicate the presence of clay-sized RD particles in the 0-0.05 m layer interfering in the results.

Discussion

The ammonium oxalate (AO) solution selectively dissolves the pedogenic, short-range crystalline (amorphous) phases of Fe and Al in the soil; nevertheless, it may also partially dissolve Fe from magnetite from lithogenic particles if they are fine grained (Rennert, 2018). Therefore, the amount of Fe_o, Al_o, Fe_d and Al_d in RD alone was also determined (Table 2) and proportionally discounted from the T1 samples.

The amorphous phases of Fe (Fe_o) and Al (Al_o) showed an increase as a result of RD application (T1) in the 0-0.05 m layer, as well as of Al_o phases in the 0.05-0.10 m. An increase in Fe_o and Al_o was also observed by Silva et al. (2021) using this same RD filled into litter bags and buried during 378 days into this same soil in the field and under three land uses (corn crop, pasture, and forest). However, statistical significance could not be assessed in that exploratory setup due to the lack of field replications.

The Fe_o accounted for 6 %, and Al_o for 27 % of the amount of Fe (1.86 g) and Al (1.16 g) in the 18.40 g of RD applied to each column. Aluminum was much more mobilized during the weathering, since the Al_t / Fe_t mass ratio (in the RD, 11.90 % Al_2O_3 = 6.30 % Al and 14.45 % Fe_2O_3 = 9.83 % Fe) was 0.6 while the ratio of the increase (T1-T0) of $Al_{o0-0.-5\,m}$ / $Fe_{o0-0.05}$ m was 1.2 (0.16 /0.13)(Table 2).

The main source of lithogenic Al was the in plagioclases, while for Fe it was pyroxenes and in Fe oxides, such as magnetite and ilmenite,which are more resistant to weathering. Plagioclases and pyroxenes are more susceptible to weathering than the Fe oxides. Because Al and Fe are located in different minerals, it is impossible to estimate the weathering level of each mineral (Lewis et al., 2021; Lino and Vlach, 2021).

In this study, the RD was applied on the column surface, and we disregarded the possibility of particulate migration to the 0.05-0.10 m layer based on the lack of increase in its Fe_o content. The subtle changes in the spectral MIR patterns may challenge this assumption (see below); however, the amount of Al leached from the columns was greater than the amount of Fe (Figure 2A and B; Table 3), further supporting the assumption of Al and Fe mobility in the soluble, not in particulate state. Finally, Al mobility was significantly enhanced in the pH values of the soil columns, around 4.5 (Table 4).

Although the contribution of RD dissolution did not modify the total mass of leached Al and Fe (Table 3), Figure 2A and B show that in the first leaching event, Al and Fe were greater in T1 as compared to T0, suggesting that most amorphous phases precipitated in the initial steps of RD weathering. This effect was observed in another similar work (Xiao et al., 2016). Another study using reactive transport modelling (RTM) predicted the formation of amorphous $Al(OH)_3$ as the secondary mineral sink for Al, reducing Al concentration in the soil solution (Lewis et al., 2021).

During the first 10 leaching events, overall concentration of elements was greater, as inferred from the EC values (Figure 2D) for columns in both T0 and T1 as compared to the leaching events from 11 to 24. This stage should refer to the freshness of lithogenic mineral surfaces and also to the system rearrangement to the experimental conditions, considering the disruption effect caused by the sampling procedure in the soil system in the field (porous network, microbiome, organic matter mineralization, etc.).

The soil material must have had established a new quasi-equilibrium state under the experimental conditions (no plants, 45 °C temperature, moisture regime, etc.). This new state seems to be achieved after the 10th leaching event; thus, extrapolation of our results to the field conditions should be done with caution. Again, most of these newly precipitated phases should have formed in the first weeks of the experiment because the leaching of Al and Fe was greater.

Another aspect that should be accounted for is the Al substitution for Fe in iron oxides. An unknown amount of Al_o may have originated from the dissolution of amorphous Fe phases. The Al ion substitutes largely (up to 33 mol % in goethites, for example) for Fe in iron oxides (e.g., Pohl et al., 2018), whereas Fe does not substitute for Al in aluminum oxides (Schwertmann, 1964).

The XRD pattern did not show a conclusive change between treatments (Figure 3A and B), possibly due to the very-short-range crystallinity and the small amount of the precipitated phases. In addition, changes in the intensity of diffracted X-rays are influenced by several factors, not only by the amount of the diffracting phase in the sample (Ali et al., 2022).

In VIS-NIR, the subtle changes in spectral signals of Fe oxides in T1 as compared to T0 suggests the presence of amorphous Fe phases in T1 (Figure 4), in accordance to the Fe_o results (Table 2) (Baldridge et al., 2009).

Ferrihydrite could be a reasonable candidate for the newly precipitated Fe phase since its spectral behavior is similar to that of goethite (reflectance in 490 and 970 nm; Coblinski et al., 2020); however, its crystal structure is less organized (short-ranged crystallinity). If the newly precipitated Fe phase was ferrihydrite, it was not detected by XRD due to lack of crystallinity and/or to the small amount precipitated (Ali et al., 2022; Cudennec and Lecerf, 2006). Moreover, Fe may also precipitate onto the surface of colloid particles in the soil. These two pools are not mutually exclusive. Also, phyllosilicate particles in the clay size range possibly increase to a specific limit size, and from that size, it is energetically more favorable for the precipitating ions to nucleate a new particle rather than contributing to the growth of a previous particle (Meunier, 2006). Due to the greater abundance of crystal defects in the oxide phases than in the phyllosilicates, this mechanism may be even more pronounced in the Fe and Al oxides.

The MIR and XRD analyses were inconclusive to identify new phases of Al oxides, even after Fe oxide was removed. Despite the high amounts of Al_o, few changes were observed in the spectra related to Al-OH bonds in the MIR scans (Figure 5). This finding corroborates the previous interpretation in which the increase in Al_o measured into the AO extracts possibly had contribution of isomorphous substitution of Al into Fe oxides. In addition, the newly precipitated Al could be partially allocated to the growth of existing gibbsite in the soil.

Because of the incongruent dissolution, elements other than Si and Al, particularly Na and Ca, reached the solution phase during the dissolution of plagioclase and Mg from pyroxenes (Lewis et al., 2021). The occurrence of such a mechanism was reinforced by the significant difference in the total element content between the soil and RD (Table 1) and the small soil CEC values (both effective and potential) (Table 4), which in turn should maintain low activity of these ions in the solution, causing the greater total mass of Ca, Na, and Mg in the leachate in T1 (Table 3). The abundance and solubility of Ca sources increased Ca in both the leached solution and the exchangeable complex; however, Mg was preferentially leached, possibly because Mg lost competition with Ca for exchangeable surfaces.

The Na content in RD was approximately two-fold the K content; however, most of the Na was released from RD leached since the exchangeable Na did not increase. The comparison between the partitioning of Na and K was impossible because the added fertilizer acted as a additional source of K. According to Lino and Vlach (2021), plagioclases have an average of 6 % Na_2O. If this plagioclase is the sole source of Na in the RD, the difference in the amount of leached Na in T1 compared to the control T0 implies 0.06 g of plagioclase weathered.

The large amount of K leached was due to the application of KCl fertilizer to the soil in the field. As a consequence of the amount of K added as a fertilizer, the total K leached and exchangeable K were not affected by the presence of RD. Again, the great K concentration in the solution, along with evaporation of soil water at the surface of the columns (maintained at 45 °C), may have caused the increase in K concentration in the 0-0.05 m layer. This mechanism appears to have occurred in both treatments since the 0-0.05 m layer had greater exchangeable K as compared to the 0.05-0.10 m layer. The low exchangeable Ca must be due to its displacement by the abundant K in the solution.

The CEC and CEC_{ef} of the soil in the columns remained unchanged despite the newly precipitated oxides, which agrees with the inference that the amount of these newly formed colloids was small. Studies on agricultural usage of RD silicate report an increase in the CEC after applying high amounts of RD (Swoboda et al., 2022). However, in addition to the higher rates applied, the authors reported an increase in the soil pH; therefore, the increase in the pH-dependent soil charges contributed to the increase in the CEC. Ramos et al. (2020), in a short-term experiment, observed a relevant reduction in exchangeable Al and an increase of CEC and the soil pH after application of different RD doses (0.9, 1.8, 3.6 and 7.2 Mg ha^{-1}). Nevertheless, it is essential to choose the more appropriate method to measure soil CEC and avoid overestimation of values (Santos et al., 2024).

The newly precipitated Fe- and Al- phases in T1 may have increased the retention of P in T1, which explains why a smaller amount of P was leached in T1. In addition, both P and Si may sorb onto the Fe- and Al- oxide surfaces, competing for the same active sites. However, Si has an advantage in this competition only at a high pH, which was not this case (Schaller et al., 2021; Schaller et al., 2022). Fertilization using Si could be used to reduce the need for the application P fertilizer due to the mobilization of unavailable P by the silicic acid.

These findings show that amorphous Al and Fe precipitate in the soil due to the weathering of primary minerals following the application of mafic RD. Thus, there is no increase in exchangeable Al, which is toxic to plants, despite the high concentrations of Al_2O_3 in the composition of the rocks. In addition, this study allowed to carry out more specific and detailed investigations into the effect of RD on CEC and the relationship with increased P levels.

Therefore, applying mafic RD in columns filled with an Oxisol increased in Fe and Al contents extracted by ammonium oxalate and changed the VIS-NIR spectra of the clay fraction in the soil after RD application compared to those in the control. Despite the amount of Al and Fe added to the soil by RD, the exchangeable and leached forms did not increase. These results were interpreted as the precipitation of newly formed, short-range crystalline (amorphous) Fe and Al oxides.

Changes in the MIR, VIS, and NIR spectra and XRD scans were subtle and inconclusive, since the signal-noise ratio of the newly precipitated phases was small due to both the great dilution of RD into the soil and to the small crystallinity range of the newly precipitated phases in the case of XRD.

Acknowledgments

The authors wish to thank the Conselho Nacional de Desenvolvimento Científico e Tecnológico (CNPq) for financial support (process 406600/2013-9) and grants (process 304660/2016-7).

Authors' Contributions

Conceptualization: Silva RC, Guimarães CCB, Azevedo AC. **Data curation:** Silva RC, Guimarães CCB, Demattê JAM, Azevedo AC. **Formal analysis:** Silva RC, Alves MMR, Demattê JAM. **Funding acquisition:** Azevedo AC. **Investigation:** Silva RC, Azevedo AC. **Methodology:** Silva RC, Guimarães CCB, Alves MMR. **Project administration:** Azevedo AC. **Resources:** Demattê JAM, Azevedo AC. **Software:** Silva RC, Guimarães CCB, Azevedo AC. **Supervision:** Azevedo AC. **Visualization:** Silva RC. Alves MMR. Demattê JAM. **Writing-original draft:** Silva RC, Azevedo AC. **Writing-review & editing:** Silva RC, Guimarães CCB, Alves MMR, Demattê JAM, Azevedo AC.

References

Ali A, Chiang YW, Santos RM. 2022. X-ray diffraction techniques for mineral characterization: a review for engineers of the fundamentals, applications, and research directions. Minerals 12: 205. https://doi.org/10.3390/min12020205

Baldridge AM, Hook SJ, Grove CI, Rivera G. 2009. The ASTER spectral library version 2.0. Remote Sensing of Environment 113: 711-715. https://doi.org/10.1016/j.rse.2008.11.007

Coblinski JA, Giasson É, Demattê JAM, Dotto AC, Costa JJF, Vašát R. 2020. Prediction of soil texture classes through different wavelength regions of reflectance spectroscopy at various soil depths. Catena 189: 104485. http://doi.org/10.1016/j.catena.2020.104485

Coblinski JA, Inda AV, Dematte JAM, Dotto AC, Gholizadeh A, Giasson E. 2021. Identification of minerals in subtropical soils with different textural classes by VIS-NIR-SWIR reflectance spectroscopy. Catena 203: 105334. https://doi.org/10.1016/j.catena.2021.105334

Cudennec Y, Lecerf A. 2006. The transformation of ferrihydrite into goethite or hematite, revisited. Journal of Solid State Chemistry 179: 716-722. https://doi.org/10.1016/j.jssc.2005.11.030

Day PR. 1965. Particle fractionation and particle-size analysis. In: Black CA. eds. Methods of soil analysis, Part 1: Physical and mineralogical properties, including statistics of measurement and sampling. American Society of Agronomy, Madison, WI, USA. https://doi.org/10.2134/agronmonogr9.1.c43

Fisher BA, Yoo K, Aufdenkampe AK, Nater EA, Feinberg JM, Nyquist JE. 2022. Mineral surface area in deep weathering profiles reveals the interrelationship of iron oxidation and silicate weathering, Earth Surface Dynamics 11: 51-69. https://doi.org/10.5194/esurf-2022-9

Food and Agriculture Organization of the United Nations [FAO]. 2021. World Food and Agriculture: Statistical Yearbook. FAO, Rome, Italy.

Frank HT, Gomes MEB, Formoso MLL. 2009. Review of the areal extent and the volume of the Serra Geral Formation, Paraná Basin, South America. Pesquisas em Geociências 36: 49-57. https://doi.org/10.22456/1807-9806.17874

Gillman GP. 1979. A proposed method or the measurement of exchange properties of highly weathered soils. Australian Journal of Soil Research 17: 129-139. https://doi.org/10.1071/SR9790129

Guimarães CCB, Dematte JAM, Azevedo AC, Dalmolin RSD, ten Caten, A, Sayão VM, et al. 2021. Soil weathering behavior assessed by combined spectral ranges: Insights into aggregate analysis. Geoderma 402: 115154. https://doi.org/10.1016/j.geoderma.2021.115154

Hahn A, Vogel H, Andó S, Garzanti E, Kuhn G, Lantzsch H, et al. 2018. Using Fourier transform infrared spectroscopy to determine mineral phases in sediments. Sedimentary Geology 375: 27-35. https://doi.org/10.1016/j.sedgeo.2018.03.010

Laxen DPH, Harrison RM. 1981. Cleaning methods for polythene containers prior to the determination of trace metals in fresh water samples. Analytical Chemistry 53: 345-350. https://doi.org/10.1021/ac00225a051

Lewis AL, Sarkar B, Wade P, Kemp SJ, Hodson ME, Taylor LL, et al. 2021. Effects of mineralogy, chemistry and physical properties of basalts on carbon capture potential and plant-nutrient element release via enhanced weathering. Applied Geochemistry 132: 105023. https://doi.org/10.1016/j.apgeochem.2021.105023

Lino LM, Cavallaro FA, Vlach SRF, Coelho DC. 2018. 2D magnetometric modeling of a basic-intermediate intrusion geometry: geophysical and geological approaches applied to the Limeira intrusion, Paraná Magmatic Province (SP, Brazil). Brazilian Journal of Geology 48: 305-315. https://doi.org/10.1590/2317-4889201820180099

Lino LM, Vlach SRF. 2021. Textural and geochemical evidence for multiple, sheet-like magma pulses in the Limeira intrusion, Paraná Magmatic Province, Brazil. Journal of Petrology 62: 1-38. https://doi.org/10.1093/petrology/egab011

Mehra OP, Jackson ML. 1958. Iron oxide removal from soils and clays by a dithionite-citrate system buffered with sodium bicarbonate. Clays and Clay Minerals 7: 317-327. https://doi.org/10.1016/b978-0-08-009235-5.50026-7

Meunier A. 2006. Why are clay minerals small?. Clay Minerals 41: 551-566. https://doi.org/10.1180/0009855064120205

Mohanty B, Gupta A, Das BS. 2016. Estimation of weathering indices using spectral reflectance over visible to mid-infrared region. Geoderma 266: 111-119. https://doi.org/10.1016/j.geoderma.2015.11.030

Park J, Yoon S, Lee H, An J, Nam K. 2024. Effects of in situ Fe oxide precipitation on As stabilization and soil ecological resilience under salt stress. Journal of Hazardous Materials 462: 132629. https://doi.org/10.1016/j.jhazmat.2023.132629

Pohl L, Kölbl A, Werner F, Mueller CW, Höschen C, Häusler W, et al. 2018. Imaging of Al/Fe ratios in synthetic Al-Goethite revealed by nanoscale secondary ion mass spectrometry. Rapid Communications in Mass Spectrometry 32: 619-628. https://doi.org/10.1002/RCM.8088

Ramos CG, Medeiros DS, Gomez L, Oliveira LFS, Schneider IAH, Kautzmann RM. 2020. Evaluation of soil re-mineralizer from by-product of volcanic rock mining: experimental proof using black oats and maize crops. Natural Resources Research 29: 1583-1600. https://doi.org/10.1007/s11053-019-09529-x

Rennert T. 2018. Wet-chemical extractions to characterise pedogenic Al and Fe species – a critical review. Soil Research 57: 1-16. https://doi.org/10.1071/SR18299

Ramaroson VH, Becquer T, Sá SO, Razafimahatratra H, Delarivière JL, Blavet D, et al. 2018. Mineralogical analysis of ferralitic soils in Madagascar using NIR spectroscopy. Catena 168: 102-109. https://doi.org/10.1016/j.catena.2017.07.016

Santos HG, Carvalho Júnior W, Dart RO, Áglio MLD, Sousa, JS, Pares JG, et al. 2011. The New Soil Map of Brazil: Updated Legend = O Novo Mapa de Solos do Brasil: Legenda Atualizada. Embrapa Solos, Rio de Janeiro, RJ, Brazil (in Portuguese).

Santos RA, Reis BR, Azevedo AC, Sermarini RA. 2024. Potential errors in cation exchange capacity measurement in soils amended with rock dust: two case studies. Communications in Soil Science and Plant Analysis 55: 329-342. https://doi.org/10.1080/00103624.2023.2268650

Schaller J, Puppe D, Kaczorek D, Ellerbrock R, Sommer M. 2021. Silicon cycling in soils revisited. Plants 10: 295. https://doi.org/10.3390/plants10020295

Schaller J, Wu B, Amelung W, Hu Z, Stein M, Lehndorff E, et al. 2022. Silicon as a potential limiting factor for phosphorus availability in paddy soils. Scientific Reports 12: 16329. https://doi.org/10.1038/s41598-022-20805-4

Schwertmann U. 1964. Differentiation of the iron oxides of the soil by photochemical extraction with acidic ammonium oxalate solution = Differenzierung der eisenoxide des bodens durch photochemische extraktion mit ammoniumoxalat-lösung. Journal of Plant Nutrition and Soil Science 105: 194-202 (in German). https://doi.org/10.1002/jpln.3591050303

Silva RC, Cury ME, Ieda JJC, Sermarini RA, Azevedo AC. 2017. Chemical attributes of a remineralized Oxisol. Ciência Rural 47: e20160982. https://doi.org/10.1590/0103-8478cr20160982

Silva RC, Ferreira EP, Azevedo AC. 2021. Weathering features of a remineralizer in soil under different land uses. Pesquisa Agropecuária Brasileira 56: e01442. https://doi.org/10.1590/S1678-3921.pab2021.v56.01442

Slessarev EW, Chadwick OA, Sokol NW, Nuccio EE, Pett-Ridge J. 2021. Rock weathering controls the potential for soil carbon storage at a continental scale. Biogeochemistry 157: 1-13. https://doi.org/10.1007/S10533-021-00859-8

Soil Survey Staff. 1999. Soil Taxonomy: A Basic System of Soil Classification for Making and Interpreting Soil Surveys. 2ed. USDA-NRCS, Washington, DC, USA.

Soil Survey Staff. 2014. Soil Survey Field and Laboratory Methods Manual. 2ed. USDA-NRCS, Washington, DC, USA.

Swoboda P, Döring TF, Hamer M. 2022. Remineralizing soils? The agricultural usage of silicate rock powders: a review. Science of The Total Environment 807: 150976. https://doi.org/10.1016/j.scitotenv.2021.150976

Terra FS, Demattê JAM, Viscarra-Rossel RA. 2018. Proximal spectral sensing in pedological assessments: vis-NIR spectra for soil classification based on weathering and pedogenesis. Geoderma 318: 123-136. https://doi.org/10.1016/j.geoderma.2017.10.053

van Raij B, Andrade JC, Cantarella H, Quaggio JA. 2001. Chemical Analysis to Evaluate the Fertility of Tropical Soils = Análise Química para Avaliação da Fertilidade de Solos Tropicais. Instituto Agronômico, Campinas, SP, Brazil (in Portuguese).

Vienne A, Poblador S, Portillo-Estrada M, Hartmann J, Ijiehon S, Wade P, et al. 2022. Enhanced weathering using basalt rock powder: carbon sequestration, co-benefits and risks in a mesocosm study with *Solanum tuberosum*. Frontiers in Climate 4: 869456. https://doi.org/10.3389/fclim.2022.869456

Wang F, Dreisinger D, Jarvis M, Hitchins T. 2019. Kinetics and mechanism of mineral carbonation of olivine for CO_2 sequestration. Minerals Engineering 131: 185-197. https://doi.org/10.1016/j.mineng.2018.11.024

Xiao L, Sun Q, Yuan H, Li X, Chu Y, Ruan Y, et al. 2016. A feasible way to increase carbon sequestration by adding dolomite and K-feldspar to soil. Cogent Geoscience 2: 1205324. https://doi.org/10.1080/23312041.2016.1205324

Zhang S, Bai X, Zhao C, Tan Q, Luo G, Wang J, et al. 2021. Global CO_2 consumption by silicate rock chemical weathering: its past and future. Earth's Future 9: e2020EF001938. https://doi.org/10.1029/2020EF001938